

# Analysis of an atom laser based on the spatial control of the scattering length

Alicia V. Carpentier, Humberto Michinel, and María I. Rodas-Verde

Área de Óptica, Facultade de Ciencias de Ourense, Universidade de Vigo, As Lagoas s/n, Ourense, ES-32004 Spain

Víctor M. Pérez-García

Departamento de Matemáticas, ETSI Industriales, Universidad de Castilla-La Mancha, 13071 Ciudad Real, Spain

(Received 24 February 2006; published 21 July 2006)

In this paper we analyze atom lasers based on the spatial modulation of the scattering length of a Bose-Einstein condensate. We demonstrate, through numerical simulations and approximate analytical methods, the controllable emission of matter-wave bursts and study the dependence of the process on the spatial shape of the scattering length along the axis of emission. We also study the role of an additional modulation of the scattering length in time.

DOI: [10.1103/PhysRevA.74.013619](https://doi.org/10.1103/PhysRevA.74.013619)

PACS number(s): 03.75.Lm, 42.65.Jx, 42.65.Tg

## I. INTRODUCTION

Atom lasers are sources of coherent matter waves that use an ultracold gas of trapped alkali-metal atoms as a reservoir from which coherent pulses of thousands of atoms are extracted. Since the experimental achievement of Bose-Einstein condensation (BEC) in gases [1], several methods have been proposed to deliver atoms from their confinement. The first of these devices used short radio-frequency pulses as outcoupling mechanism, flipping the spins of some of the atoms to release them from the trap [2]. Later, other atom lasers were built leading to pulsed, semicontinuous, or single-atom coherent sources [3–7].

The quality of an atom laser is given by the amount of atoms that can be delivered from the trap and by the purity of the emission process. Concerning this point, it has been recently shown [8] that spin-flipping techniques present serious limitations in the number of atoms that can be emitted. This effect is related to the fluctuations at high flux due to the fact that the output-coupling mechanism populates all accessible Zeeman states. This constitutes a strong drawback for practical applications of atom lasers in high-precision measurements like matter-wave gyroscopes [9].

On the other hand, an atomic soliton laser using the mechanism of modulational instability was proposed in Ref. [10]. In this case, the emission is obtained by the combination of purely nonlinear effects in the atom cloud and the relaxation of the trap, it being necessary that the total number of particles in the cloud exceeds a critical threshold. This system has the advantage over standard atom lasers of producing matter-wave pulses in the form of *solitons* [11–13], a kind of nonlinear waves generated by a perfect balance between dispersive and nonlinear effects, yielding robust wave packets that propagate without shape distortion [14]. Other types of atom lasers based on nonlinear effects have been proposed [15].

However, although one could extract a few coherent solitons from a Bose-Einstein condensate by the mechanism of modulational instability, the final output would be very limited since the number of atoms per pulse generated by this phenomenon is only a small fraction of the initial number of atoms in the condensate due to collapse processes. Moreover, the number of solitons generated is not large and half of

them would be directed backward. Finally, the trap must be destroyed for outcoupling and the pulses travel at different speeds once the trap is removed. Thus, it is important to discuss new outcoupling mechanisms for atom lasers. This is specially interesting since the techniques for generating BECs with large numbers of particles and their physical properties are nowadays well established and the current challenges in the field concern the design of practical devices [16].

In a recent work [17] a novel outcoupling mechanism for an atom laser was proposed. The method is based on the fact that a spatial variation of the scattering length ( $a$ ) (see Fig. 1) can be used to extract a controllable train of up to several hundreds of atomic solitons from a BEC without altering the trap properties. In Ref. [17], a simple model for the spatial variation of the scattering length (a step function) was used in order to introduce the basic ideas and illustrate the phenomenon. However, for the practical realization of such a device, a deeper analysis must be done, including studying the role of more physical distributions of the spatial dependence of  $a$  and the temporal control of the output by considering an additional time dependence of the scattering length. In this paper we study in detail these aspects of the soliton

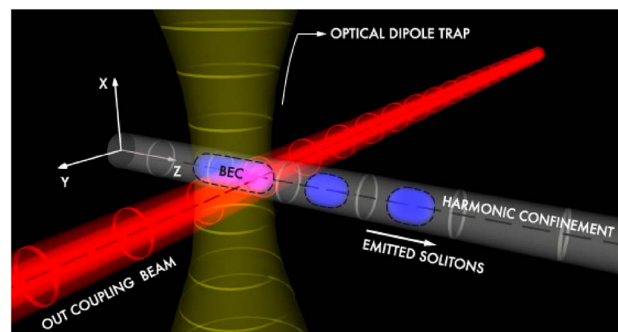


FIG. 1. (Color online) Sketch of the system we will study in this paper for the case of optically controlled scattering length showing the BEC in the optical dipole trap, the transverse magnetic confinement, and the laser beam used to manage the scattering length region. For a critical number of atoms or equivalently below a critical value of the scattering length, a burst of matter-wave solitons is emitted along the weakly confining axis.

emission process which are relevant for the theoretical understanding and experimental demonstration of this new type of atom laser.

The structure of this paper is as follows. In Sec. II, we present the configuration of the system and the mathematical model to be used for the theoretical analysis. In Sec. III we study the mechanism of emission of single solitons. To do so we first study a simplified model for which an analytical study can be done. We also analyze theoretically and numerically more realistic schemes with Gaussian-shaped spatial variations of the scattering length. In Sec. IV we have examined the problem of partial uncoupling and multisoliton emission. Finally, in Sec. V we study the effect of temporal variations of the scattering length induced by pulsed beams.

## II. SYSTEM CONFIGURATION AND THEORETICAL MODEL

As in Ref. [17], we assume a BEC that is strongly confined in the transverse directions ( $x, y$ ) and weakly along the longitudinal one ( $z$ ) leading to a *cigar-shaped* configuration. We will consider the effect of a spatial variation of the scattering length along  $z$  from positive (or zero) to negative values. In principle this can be done by magnetic [18] or optical [19] means, for instance by using an appropriate laser beam that shines along one of the edges of the condensate as in the sketch of the system plotted in Fig. 1. In this case the region of negative scattering length can be varied and displaced along the condensate by simply moving the laser beam. The variation of  $a$  can also be controlled in time by using pulsed laser beams. Similar arguments apply for the magnetically controlled scattering length, although laser tuning allows for faster and easier manipulation of the spatial variations of the scattering length. In any case the point is that we will depart from the model of steplike spatial variation of the scattering of Ref. [17] to more realistically achievable smoother dependences.

The spatial modulation of the scattering length acts as follows. The part of the cloud that overlaps the region with  $a < 0$  (shaded region of Figs. 2 and 3) decreases the strength of the confinement in this zone (see potential curves of Fig. 3) resulting in an asymmetric effective trap with a minimum shifted toward the uncoupling laser. The exact form of this new potential depends on the strength of the nonlinear effects (i.e., the product  $aN$ ,  $N$  being the number of atoms in the cloud). For values of  $aN$  large enough, the dipole trap is overcome and part of the cloud is delivered and emitted outward. When the condensate refills the gap left by the outgoing pulse the process starts again and a new soliton is emitted. This process will continue while there is a large enough remnant of atoms in the trap and will lead to a soliton burst escaping from the BEC.

Therefore, we will consider that the cloud of  $N$  equal bosons of mass  $m$  is tightly trapped in ( $x, y$ ) by a harmonic potential  $V_{\perp}$  of frequency  $\nu_{\perp}$  and weakly confined along  $z$  by the effect of an optical dipole trap  $V_z$  [20,21] that can be produced by a laser beam of a given width along  $z$  (see Fig. 1). Thus, we have

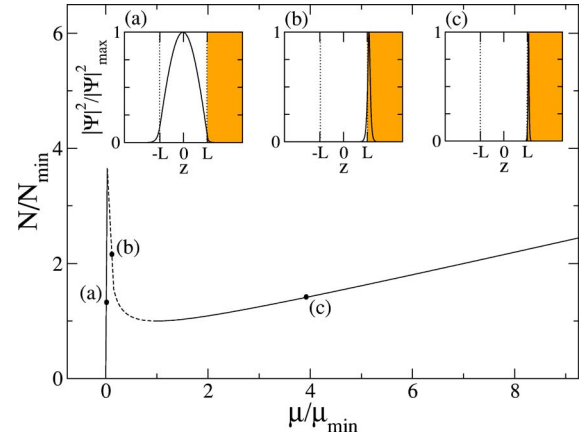


FIG. 2. (Color online) Dependence of the number of particles in the condensate  $N$  on the chemical potential  $\mu$  for the simple case of a square-shaped potential. The values are normalized by  $N_{min}$  and  $\mu_{min}$  which correspond to the minimum of the curve. For the experimental values considered in the text for  $^7\text{Li}$  we find  $N_{min} = 2 \times 10^4$  and  $\mu_{min} = \hbar v_{\perp} / 2$  for  $a = -0.3$  nm. The dashed part of the curve  $\mu(N)$  corresponds to an unstable region. The insets show the eigenmode profiles for different values of  $\mu$ , the dotted lines indicating the boundaries of the trap. The region of negative scattering length is the shaded one.

$$V(\vec{r}) = V_{\perp} + V_z = \frac{m v_{\perp}^2}{2} (x^2 + y^2) + V_0 \left[ 1 - \exp\left(-\frac{z^2}{L^2}\right) \right], \quad (1)$$

where  $V_0$  is the depth of the shallow optical dipole potential and  $L$  its characteristic width along  $z$ . The choice of a shallow Gaussian trap is very important, since the goal is to obtain uncoupling of solitons along the  $z$  axis. This can be

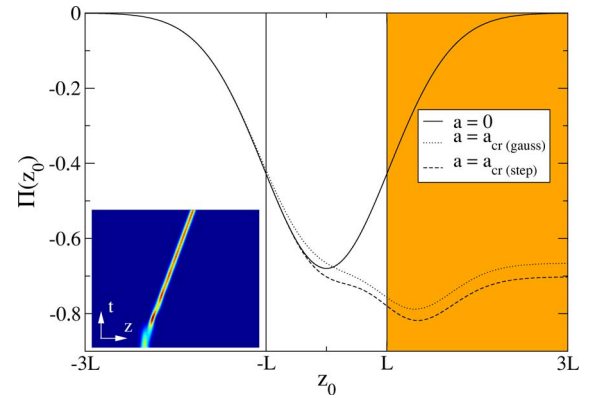


FIG. 3. (Color online) Effective potentials obtained for two different shapes of  $a(z)$ : a step function and a Gaussian+step distribution. The potentials correspond to  $a = a_{cr}$  for each form of the scattering length. The continuous line shows the effective potential for  $a = 0$  (the linear trap). The shaded zone indicates the region of negative scattering length in the step model. Inset: emission of a single soliton in the case of a Gaussian+step modulation of  $a$  (dotted curve). Time goes from  $t = 0$  to  $1000 \nu_{\perp}^{-1}$ . The spatial width of the window is  $150 r_{\perp}$ . The red false color corresponds to the maximum density of atoms and the blue to the minimum.

achieved with a potential barrier that can be overcome by the self-interaction effects. The dynamics of the previous system in the mean-field limit is described by a Gross-Pitaevskii equation of the form

$$i\hbar \frac{\partial \Psi}{\partial t} = -\frac{\hbar^2}{2m} \nabla^2 \Psi + V(\vec{r})\Psi + U(z)|\Psi|^2\Psi, \quad (2)$$

where  $\Psi$  is the condensate wave function, and its norm  $N = \int |\Psi|^2 d^3\mathbf{r}$  gives the number of particles. The coefficient  $U(z) = 4\pi\hbar^2 a(z)/m$  depends on the scattering length  $a$ , which characterizes the two-body interactions between atoms. As commented previously, we will consider  $a$  to be a function of  $z$  with a localized region in which it becomes negative.

We will concentrate on situations in which the spatial size of the ground state of the optical dipole trap is much larger than that of the ground state of the transverse harmonic potential leading to effectively one-dimensional dynamics. In this situation we can describe the dynamics of the condensate in the quasi-one-dimensional limit as given by a factorized wave function of the form [11]  $\Psi(\mathbf{r}, t) = \Phi_0(x, y)\psi(z, t)$ , satisfying

$$i \frac{\partial \psi}{\partial \tau} = -\frac{r_\perp^2}{2} \frac{\partial^2 \psi}{\partial z^2} + f(z)\psi + g|\psi|^2\psi, \quad (3)$$

where  $r_\perp = \sqrt{\hbar/m\nu_\perp}$  is the transverse size of the cloud,  $f(z) = V_z/(\hbar\nu_\perp)$ ,  $\tau = \nu_\perp t$  is the time measured in units of the inverse of the radial trapping frequency, and  $g(z) = 2\pi r_\perp^2 a(z)$  is the effective interaction coefficient.

As an example we will present specific numbers in this paper corresponding to  $^7\text{Li}$ , using the experimental parameters of Ref. [12],  $V_0 = \hbar\nu_\perp/2$ ,  $\nu_\perp = 1$  kHz,  $L = 4r_\perp$ ,  $N = 3 \times 10^5$ ,  $w = 5.4r_\perp$ ,  $a = -1.4$  nm, and times ranging from  $t = 0$  to 1 s. However, our results hold for different atomic species like  $^{85}\text{Rb}$  and  $^{133}\text{Cs}$ , with adequate parameters.

### III. SINGLE-SOLITON EMISSION

#### A. Exact theory for square potentials

As we have pointed out before, we will consider a situation in which the scattering length is changed in a localized region near the edge of the optical trap. In that case, it is possible to understand the basics of the phenomenon of the emission of a single soliton using a simple model. We consider a square trapping potential of width  $L$  and depth  $V_0$  and a steplike scattering length, as illustrated in Fig. 2. Mathematically

$$V(z) = \begin{cases} 0, & z < -L, \\ V_0 < 0, & -L < z < L, \\ 0, & z > L, \end{cases} \quad (4a)$$

and

$$a(z) = \begin{cases} 0, & z < L, \\ a_* < 0, & z > L. \end{cases} \quad (4b)$$

Although this model is a rough simplification of the more realistic situations to be described in detail later on, it cap-

tures the big picture of the process. In fact, from the experimental point of view it will be simpler to have  $a > 0$  instead of  $a = 0$  in the confining zone. This is because setting  $a = 0$  needs the addition of an extra magnetic field. However, we have checked that the effect of a positive scattering length in the confining zone is only to slightly reduce the confinement. This yields a lower threshold in the emission and the same qualitative behavior as in the case of  $a = 0$ . The previous model can be solved analytically, by simply calculating the solution of the Schrödinger equation in the three zones. Defining  $\gamma_1 = 2\mu/r_\perp \hbar\nu_\perp$ ,  $\gamma_2 = 2(\mu - V_0)/r_\perp \hbar\nu_\perp$ , and  $\gamma_3 = 2\mu/r_\perp \hbar\nu_\perp$ , we get

$$\Psi(z) = \begin{cases} A_1 \exp(-\gamma_1 z), & z < -L, \\ A_2 \cos[(z - z_2)\gamma_2], & -L < z < L, \\ A_3 \operatorname{sech}[(z - z_3)\gamma_3], & z > L. \end{cases} \quad (5)$$

As can be appreciated in the insets of Fig. 2, the shape of the wave function depends on  $a_*$ . Thus, a potential connected to a region where atom-atom interactions are activated displays a continuum of stationary fundamental states. For values of  $a_*$  close to zero, (or equivalently a low number of atoms  $N$  in the BEC), the cloud is located at the center of the trap. As the product  $Na_*$  is increased, the center of the cloud is displaced toward the boundary between zones 2 and 3. For higher values of  $Na_*$ , the cloud is completely located in the region with  $a < 0$  and takes the form of a soliton with a hyperbolic secant profile. The continuity of the wave function of the condensate and its derivatives at the boundaries between the three regions yields the following relationships:

$$z_2 = -\left[ L + \frac{1}{\gamma_2} \tan^{-1}\left(\frac{-\gamma_1}{\gamma_2}\right) \right], \quad (6a)$$

$$z_3 = L - \frac{1}{\gamma_3} \tanh^{-1}\left(\frac{\gamma_2}{\gamma_3} \tan[\gamma_2(L - z_2)]\right), \quad (6b)$$

$$A_1 = A_3 \operatorname{sech}[\gamma_3(L - z_3)] \operatorname{sech}[\gamma_2(L - z_2)], \quad (6c)$$

$$A_2 = A_1 \cos[-\gamma_2(L + z_2)] e^{\gamma_1 L}, \quad (6d)$$

$$A_3 = \frac{1}{\operatorname{sech} z} \sqrt{\frac{2 \operatorname{sech}^2 z - 2\mu/r_\perp^2 \hbar\nu_\perp + 1}{\sqrt{8\pi r_\perp a_*}}}. \quad (6e)$$

The number of atoms  $N$  in the stationary state can be easily calculated by integrating  $|\psi|^2$  over  $z$ ,

$$N = \frac{A_2^2}{2\gamma_1} \exp(-2\gamma_1 L) + \frac{A_3^2}{\gamma_3} \{1 - \tanh[\gamma_3(L - z_3)]\} + \frac{A_1^2}{2} \left( 2L + \frac{\sin(2\gamma_2 L) \cos(2\gamma_2 z_2)}{\gamma_2} \right). \quad (7)$$

The previous equation provides the dependence of the chemical potential of the ground state on the number of atoms. As can be seen in Fig. 2 the curve  $N$  vs  $\mu$  for all the stationary ground states has one maximum and one minimum, and displays a negative slope between them. It is well known from the theory of nonlinear Schrödinger equations

[22,23] that the stationary states corresponding to the zone with  $dN/d\mu < 0$  are unstable; this is known as the Vakhitov-Kolokolov criterion of stability. This fact implies that any small perturbation will affect dramatically the eigenstates in this zone, which are basically nonlinear surface waves located in the boundary between the linear potential and the nonlinear region. As a consequence of this instability, the surface wave is reflected by the boundary and emitted to the nonlinear zone.

### B. Approximate theory for realistic potentials

The analysis of the previous section, although exact, is only a crude representation of the real potentials which can be used in experimental scenarios. To study more physical spatial distributions of  $a$  we will combine the use of numerical methods with approximate averaged Lagrangian formalisms [24] consisting in minimizing the Lagrangian density over a family of trial wave functions which we will choose as

$$\psi(z, \tau) = A \exp\left(-\frac{(z - z_0(\tau))^2}{2w^2}\right) \exp[iv(\tau)z]. \quad (8)$$

This ansatz leaves a single free degree of freedom for the atom cloud: its center  $z_0(\tau)$ , which moves with speed proportional to  $v(\tau)$ .

To study a scenario close to a possible experimental setup in which the scattering length is optically managed, we will analyze the soliton emission when the laser beam used to manage the scattering length takes the form

$$a(z) = \begin{cases} a \exp\left[-\left(\frac{z-D}{w_g}\right)^m\right], & z < D + w_g, \\ a, & z > D + w_g, \end{cases} \quad (9)$$

i.e., a hyper-Gaussian ramp connected at its maximum to an infinite plateau. This choice allows us to cover many cases between the two limits  $m=2$  corresponding to a Gaussian distribution and  $m \rightarrow \infty$  representing a step function. The standard calculations taking  $a(z)$  as given by Eq. (9) lead to a Newton-type equation of the form

$$\ddot{z}_0 = -\frac{d\Pi}{dz_0}, \quad (10a)$$

where  $\Pi(z_0)$  is given by

$$\begin{aligned} \Pi(z_0) = r_{\perp}^2 & \left[ \frac{V_0}{\hbar v_{\perp}} \left( 1 - \frac{e^{-z_0^2/(w^2+L^2)}}{\sqrt{1+w^2/L^2}} \right) \right. \\ & \left. + \frac{N}{2w^2\pi} \int_{-\infty}^{\infty} \exp\left(\frac{-2(z-z_0)}{w^2}\right) a(z) dz \right]. \end{aligned} \quad (10b)$$

From Eq. (10a) we see that the center of gravity of the cloud ( $z_0$ ) behaves like a classical particle under the effect of a potential  $\Pi(z_0)$ . This provides a qualitative understanding of the soliton emission: for the linear case ( $a=0$ ) the center of the cloud is located at the bottom of the Gaussian trap and approximates its fundamental eigenstate [Fig. 2(a)]; as  $a$

takes more negative values the effective trapping of the cloud is deformed and the minimum of the equivalent potential moves to the region with  $z > 0$ .

The calculations in the particular cases of  $m=2$ —a Gaussian beam—and  $m \rightarrow \infty$ —a step function—lead us to the effective potentials

$$\begin{aligned} \Pi_g(z_0) = r_{\perp}^2 & \left( \frac{V_0}{\hbar v_{\perp}} \left( 1 - \frac{e^{-z_0^2/(w^2+L^2)}}{\sqrt{1+w^2/L^2}} \right) \right. \\ & \left. + \frac{aN}{w\sqrt{2\pi}} \left\{ \operatorname{erfc}\left(\frac{\sqrt{2}(D-z_0)}{w}\right) + \frac{w_g}{\sqrt{w_g^2+w^2/2}} \right. \right. \\ & \times \exp\left(-\frac{(D-z_0)^2}{w_g^2+w^2/2}\right) \\ & \times \left[ \operatorname{erf}\left(\frac{-2z_0w_g+2w_gD+2w_g^2+w^2}{w\sqrt{2w_g^2+w^2}}\right) \right. \\ & \left. \left. - \operatorname{erf}\left(\frac{-2z_0w_g^2-Dw^2}{w_gw\sqrt{2w_g^2+w^2}}\right) \right] \right\} \right), \end{aligned} \quad (11a)$$

$$\begin{aligned} \Pi_s(z_0) = \frac{\sqrt{\pi}}{2} r_{\perp}^2 & \left[ \frac{V_0}{\hbar v_{\perp}} \left( 1 - \frac{e^{-z_0^2/(w^2+L^2)}}{\sqrt{1+w^2/L^2}} \right) \right. \\ & \left. + \frac{1}{\sqrt{2\pi}} \frac{aN}{w} \operatorname{erfc}\left(\frac{\sqrt{2}(D-z_0)}{w}\right) \right], \end{aligned} \quad (11b)$$

where  $g$  and  $s$  refer, respectively, to the step and Gaussian ramps. The functions  $\operatorname{erfc}(u)$  and  $\operatorname{erf}(u) = \frac{2}{\sqrt{\pi}} \int_0^u \exp(-v^2) dv = 1 - \operatorname{erfc}$  are the complementary error and the error functions, respectively. Figure 3 shows the equivalent potentials  $\Pi$  given by Eqs. (11a) and (11b) for different values of  $a$ . As the scattering length becomes more negative, it reaches a limiting value  $a_{cr}$  for which the potential  $\Pi(0) = \Pi(\infty)$ ; thus if the atom cloud is initially placed at  $z_0=0$  it will oscillate around the minimum and escape  $z_0(\tau) \rightarrow \infty$  for  $\tau \rightarrow \infty$ , a phenomenon that is called soliton emission [25]. The critical value of  $a$  that corresponds to the threshold for soliton emission can be obtained within our formalism from the condition  $\Pi(0) = \Pi(\infty)$ , which leads to

$$\begin{aligned} Na_{cr}^g = \frac{V_0w\sqrt{2\pi}}{\hbar v_{\perp}\sqrt{1+w^2/L^2}} & \left( \left\{ \frac{1}{\sqrt{2}} \operatorname{erfc}\left(\frac{D+w_g\sqrt{2}}{w}\right) \right. \right. \\ & \left. \left. + \frac{w_g}{\sqrt{2w_g^2+w^2}} \exp\left(\frac{-2D^2}{2w_g^2+w^2}\right) \right. \right. \\ & \times \left[ \operatorname{erf}\left(\frac{-2w_gD+2w_g^2+w^2}{w\sqrt{2w_g^2+w^2}}\right) \right. \\ & \left. \left. - \operatorname{erf}\left(\frac{-Dw}{w_g\sqrt{2w_g^2+w^2}}\right) \right] \right\} - \frac{2}{\sqrt{2}} \right)^{-1}, \end{aligned} \quad (12a)$$

$$Na_{cr}^s = \frac{\sqrt{2\pi}V_0}{\hbar v_{\perp}} \frac{wL}{\sqrt{L^2+w^2}} \left[ \operatorname{erfc}\left(\frac{\sqrt{2}D}{w}\right) - 2 \right]^{-1}. \quad (12b)$$

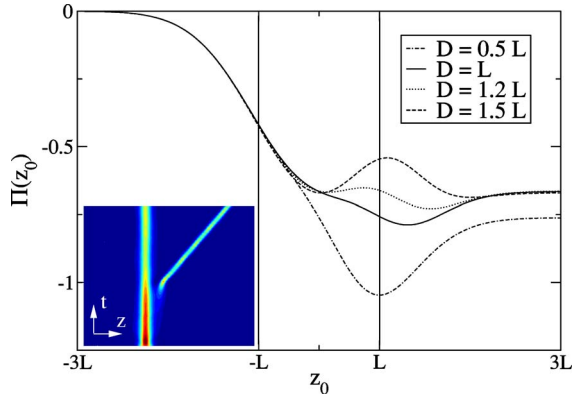


FIG. 4. (Color online) Same as Fig. 3 for the Gaussian+step distribution. The effective potentials correspond to different values of the penetration parameter  $D$ .

In both cases, it is possible to find approximate expressions that hold for  $D \approx w$  and  $V_0 = \Delta \hbar \nu_{\perp}$ , with  $\Delta < 1$ , which provides a shallow trap. Thus, it is possible to write

$$Na_{cr}^g \approx -2.655 \frac{\Delta w L}{\sqrt{L^2 + w^2}}, \quad (13a)$$

$$Na_{cr}^s \approx -2.565 \frac{\Delta w L}{\sqrt{L^2 + w^2}}. \quad (13b)$$

In order to check the validity of this approach, we have performed a numerical integration of Eq. (3) with a split-step Fourier method using as initial condition a Gaussian distribution for the cloud, which is initially located at the center of a dipole trap. We have used absorbing boundary conditions in a grid with 520 points. Adding more points to the discretization do not changed the results of the simulation. We have found a good agreement between the exact numerical value and the prediction from Eq. (13a). The variational model is more accurate for Gaussian potentials. The main discrepancy we have found after a wide numerical exploration of the parameter space is a factor  $\sqrt{2}$  that is mainly due to the choice of the ansatz.

#### IV. PARTIAL OUTCOUPLING AND MULTISOLITON EMISSION

The distance  $D$  between the edge of the region in which the scattering length varies and the center of the trap plays an important role in the emission process as shown in Fig. 4. As can be seen in the plots, there is a critical overlapping between the  $a < 0$  region and the trap, for which the effective potential shows a central maximum between two adjacent minima. In this case, part of the cloud is reflected backward by the intermediate barrier and thus it is not possible to extract the whole cloud (see inset of Fig. 4). Thus, the emission will be of higher quality in traps of width below a certain critical threshold, which can be numerically calculated from the conditions  $d\Pi/dz=0$  and  $d^2\Pi/dz^2 > 0$ .

A deeper numerical exploration based on Eq. (3) reveals interesting effects beyond those contained in the averaged

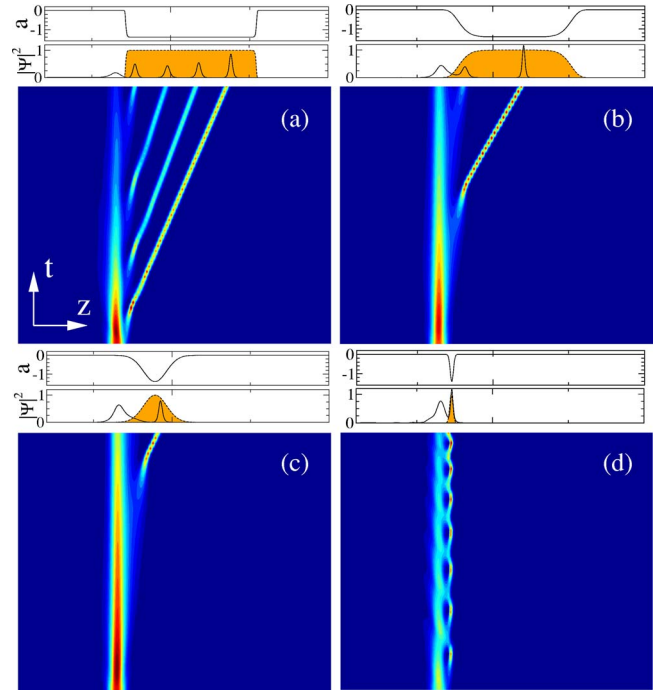


FIG. 5. (Color online) Emission of atomic solitons for different outcoupling laser beams (shaded region in the top plots) of super-Gaussian shapes with different values of the parameter  $m$ :  $m =$  (a) 100, (b) 8, (c) and (d) 2 (Gaussian distributions of different widths). The small frames in the top of each picture display  $a(z)$  and the profile of the solitons at  $t = 600\nu_{\perp}^{-1}$ . Vertical axis in bottom pictures is time from  $t = 0$  to  $600\nu_{\perp}^{-1}$ . Horizontal axis is 60 times the width  $L$  of the Gaussian trap. In all cases the product  $Na$  is eight times the value of Fig. 4. The rest of the parameters are the same as in Fig. 3.

Lagrangian description. An example is shown in Fig. 5. As  $a_*$  becomes more negative we obtain the emission of an integer number of solitons.

In this section and to approximate our analysis to realistic scenarios we have considered the scattering length to be of the form

$$a(z) = a \exp \left[ - \left( \frac{z - D}{w_g} \right)^m \right], \quad (14)$$

i.e., a super-Gaussian of finite width.

In Fig. 5 we illustrate the dependence of the emission for different shapes of the function  $a(z)$ . We begin with a profile close to the step form ( $m = 100$ ) and then we relax the shape by diminishing the value of  $m$  until we reach a Gaussian function. We have also observed that for finite  $a < 0$  regions, once the emitted solitons reach the opposite edge of the zone with negative scattering length, they are reflected backward and thus remain trapped in the vicinity of the BEC reservoir [see Figs. 5(d) and 6(a)]. This effect may have applications in the control of the emitted solitons once outcoupled and in the design of practical devices like laser tweezers for atoms [26–28].

Another interesting consideration in order to construct experimentally wide regions of negative scattering length is to use the superposition of several mutually incoherent laser

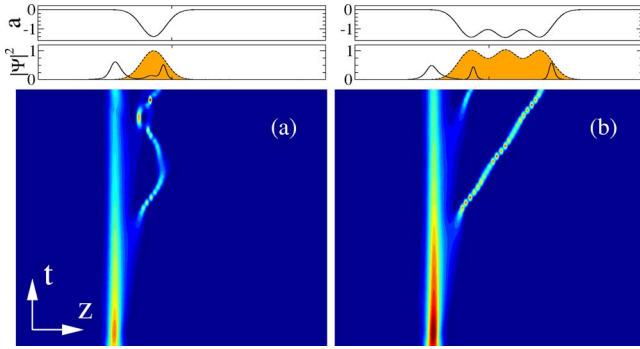


FIG. 6. (Color online) Emission obtained with the superposition of parallel Gaussian beams. In (a) the region of negative scattering length is generated by a single outcoupling beam as in Fig. 5(c). In (b) three equal Gaussian beams separated by the width of the beam are used to generate a wider region of negative scattering length. Top plots display  $a(z)$  and the output at  $t=1000\nu_{\perp}^{-1}$ . In the pictures, vertical axis is time from  $t=0$  to  $1000\nu_{\perp}^{-1}$ . The other parameters are the same as in Fig. 5(c).

beams as shown in Fig. 6. In Fig. 6(a) the region of negative scattering length is generated by a single outcoupling beam as in Fig. 5(c). As a result of the finite width of the outcoupling beam, the atomic soliton rebounds at the boundary as it is redirected backward to the reservoir. In Fig. 6(b) three equal Gaussian beams separated by the outcoupling beam width are used to generate a wider region of negative scattering length. In the pictures, the vertical axis is time from  $t=0$  to  $1000\nu_{\perp}^{-1}$ . The other parameters are the same as in Fig. 5(c).

We have also observed in the numerical simulations that the soliton emission is more efficient if the scattering length varies abruptly in space. Moreover, to avoid the return of the solitons once they have been emitted, it is desirable that the shape of the outcoupling beam be asymmetric. In the case in which laser beams are used to control the scattering length this could be achieved by partially overlapping parallel lasers. In order to generate an extended negative scattering length region, more lasers can be added or the outcoupling beam can be displaced following the motion of the emitted soliton.

## V. EFFECT OF TEMPORAL MODULATION OF THE OUTPUT

Finally, we have also studied the temporal control of the emission process by simulating the dynamics of the solitons outcoupled with pulsed beams. We have run calculations for different temporal sizes of the beams. The results are shown in Fig. 7. In these simulations we have used temporal profiles made with a Gaussian ramp connected to a flat top of variable size  $t_p$ . The spatial profiles are step functions. As can be seen in the pictures, depending on the duration of the pulse (i.e., the size of the flat top), the quality of the outcoupling varies, yielding a broadening in the profile of the solitons as the nonlinearity vanishes. In some cases the solitons can fuse after the emission. By varying the time that  $a$  is switched to a negative value, it is possible to obtain a periodic reconstruction of the individual solitons. The results are summarized in Fig. 7(c). In this simulation, the spatial profile of the outcoupling beam is a step function that is modulated in time with a Gaussian ramp connected at its maximum to a flat top of variable size that ends with a final Gaussian decay. The captions correspond to different sizes of the plateau  $t_p$  and separation between applied pulses  $t_s$ . In all cases time goes from  $t=0$  to  $500\nu_{\perp}^{-1}$ . Figure 7(a) corresponds to a continuous beam (i.e., no modulation); in Figs. 7(b) and 7(c) we applied three pulses with  $t_p=100\nu_{\perp}^{-1}$  in both cases and  $t_s=5\nu_{\perp}^{-1}$  and  $t_s=15\nu_{\perp}^{-1}$ , respectively. The rest of the parameters are the same as in Fig. 5(a).

## VI. CONCLUSIONS AND DISCUSSION

In summary, we have analyzed in detail the recently proposed mechanism for outcoupling coherent matter-wave pulses from a Bose-Einstein condensate. By using this technique it might be possible to obtain a regular and controllable emission of atomic soliton bursts that are easily extracted by an adequate choice of the control parameters.

The particular shape of the spatial dependence of the scattering length used for outcoupling the solitons does not affect essentially the emission process although it is of higher purity for sharp variations of the scattering length, and for regions of negative scattering length of finite extent the soliton

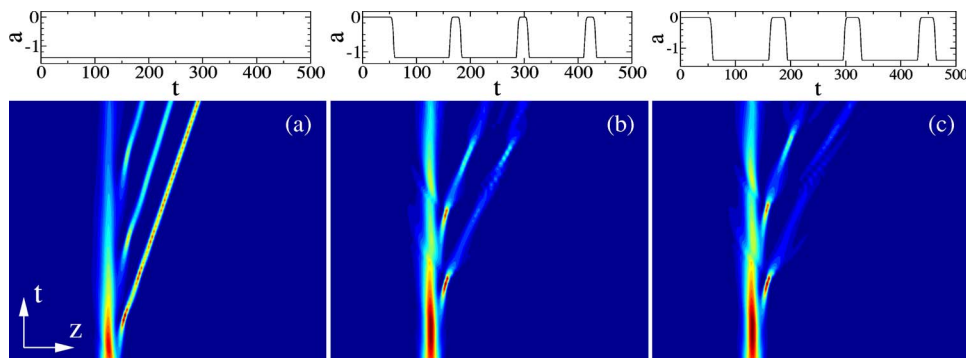


FIG. 7. (Color online) Effect of a temporal modulation in the emission process. The spatial profile of the outcoupling beam is a step function that is modulated in time with a Gaussian ramp connected at its maximum to a flat top of variable size that ends with a final Gaussian decay. The captions correspond to different sizes of the plateau  $t_p$  and separation between applied pulses  $t_s$  (plotted in the top graphs). In all cases time goes from  $t=0$  to  $500\nu_{\perp}^{-1}$ . (a) corresponds to a continuous beam (i.e., no modulation); in (b) and (c) we applied three pulses with  $t_p=100\nu_{\perp}^{-1}$  in both cases and  $t_s=5\nu_{\perp}^{-1}$  and  $15\nu_{\perp}^{-1}$ , respectively. The rest of the parameters are the same as in Fig. 5(a).

is reflected back when it reaches the boundaries. The temporal control of the solitons can be easily implemented with pulsed beams.

A warning is in order: all of our numerical predictions have been based on the one-dimensional model (3). It is well known that three-dimensional Bose-Einstein condensates with negative scattering length can collapse if the atom density is large enough [29,30]. The particular values of the critical number of atoms in the condensates and maximum atom densities depend on the specific choice of the transverse frequency  $\nu_{\perp}$ . Thus for our predictions to be valid  $\nu_{\perp}$  must be large enough to force the system to stay in the quasi-one-dimensional regime, i.e., the soliton size as described in Ref. [11] must be much larger than the typical transverse scale  $\hbar/\sqrt{m\nu_{\perp}}$ .

The management of the scattering length could be accompanied by losses when crossing a Feshbach resonance. Concerning this point we must stress that the amount of negative  $a$  necessary in our model can be achieved in  ${}^7\text{Li}$  without crossing the resonance. However, we have checked the effect of three-body inelastic collisions by adding the corresponding term to Eq. (3). The result of our simulations is that the same number of solitons are emitted for the same values of the product  $Na$  independently of the value of losses, provided they are not too high. The effect of losses is a decrease

in the number of solitons per atom, but not in the total number of solitons emitted. We believe that this behavior adds extra support to the robustness of the method.

We must stress that our results hold for different atomic species like  ${}^{85}\text{Rb}$  and  ${}^{133}\text{Cs}$ , with adequate parameters. For the case of  ${}^{133}\text{Cs}$  the scattering length can be controlled with high precision and can be made negative and large. This could provide a system in which a very high number of solitons could be generated.

Using the mechanism proposed in this paper a train of even several hundreds of solitons could be coherently out-coupled from a condensate. As the techniques for coherently feeding the remaining condensate progress, our idea could provide an outcoupling mechanism for a continuous atomic soliton laser.

#### ACKNOWLEDGMENTS

We want to acknowledge J. Brand for discussions. This work was supported by Ministerio de Educación y Ciencia, Spain (Projects No. FIS2004-02466, and No. BFM2003-02832 and network FIS2004-20188-E), Xunta de Galicia (Project No. PGIDIT04TIC383001PR), and Junta de Comunidades de Castilla-La Mancha (Project No. PAI-05-001).

- 
- [1] M. H. Anderson, J. R. Ensher, M. R. Matthews, C. E. Wieman, and E. A. Cornell, *Science* **269**, 198 (1995); K. B. Davis, M. O. Mewes, M. R. Andrews, N. J. van Druten, D. S. Durfee, D. M. Kurn, and W. Ketterle, *Phys. Rev. Lett.* **75**, 3969 (1995).
- [2] M.-O. Mewes, M. R. Andrews, D. M. Kurn, D. S. Durfee, C. G. Townsend, and W. Ketterle, *Phys. Rev. Lett.* **78**, 582 (1997).
- [3] I. Bloch, T. W. Hänsch, and T. Esslinger, *Phys. Rev. Lett.* **82**, 3008 (1999).
- [4] E. W. Hagley, L. Deng, M. Kozuma, J. Wen, K. Helmerson, S. L. Rolston and W. D. Phillips, *Science* **283**, 1706 (1999).
- [5] I. Bloch, M. Kohl, M. Greiner, T. W. Hansch, and T. Esslinger, *Phys. Rev. Lett.* **87**, 030401 (2001); M. Kohl, T. W. Hansch, and T. Esslinger, *ibid.* **87**, 160404 (2001); *Phys. Rev. A* **65**, 021606(R) (2002).
- [6] J. L. Martin, C. R. McKenzie, N. R. Thomas, D. M. Warrington, and A. C. Wilson, *J. Phys. B* **33**, 3919 (2000).
- [7] B. Mohring, M. Bienert, F. Haug, G. Morigi, W. P. Schleich, and M. G. Raizen, *Phys. Rev. A* **71**, 053601 (2005).
- [8] N. P. Robins, C. M. Savage, J. J. Hope, J. E. Lye, C. S. Fletcher, S. A. Haine, and J. D. Close, *Phys. Rev. A* **69**, 051602(R) (2004).
- [9] T. L. Gustavson, P. Bouyer, and M. A. Kasevich, *Phys. Rev. Lett.* **78**, 2046 (1997).
- [10] L. D. Carr and J. Brand, *Phys. Rev. A* **70**, 033607 (2004).
- [11] V. M. Pérez-García, H. Michinel, and H. Herrero, *Phys. Rev. A* **57**, 3837 (1998).
- [12] K. E. Strecker, G. B. Partridge, A. G. Truscott, and R. G. Hulet, *Nature (London)* **417**, 150 (2002).
- [13] L. Khaykovich, F. Schreck, G. Ferrari, T. Bourdel, J. Cubizolles, L. D. Carr, Y. Castin, and C. Salomon, *Science* **296**, 1290 (2002).
- [14] V. E. Zakharov and A. B. Shabat, *Sov. Phys. JETP* **34**, 62 (1972).
- [15] P. Y. Chen, B. A. Malomed, *J. Phys. B* **38**, 4221 (2005).
- [16] H. Ott, J. Fortagh, G. Schlotterbeck, A. Grossmann, and C. Zimmermann, *Phys. Rev. Lett.* **87**, 230401 (2001); W. Hänsel, P. Hommelhoff, T. W. Hansch, and J. Reichel, *Nature (London)* **413**, 498 (2001); **78**, 985 (1997).
- [17] M. I. Rodas-Verde, H. Michinel, and V. M. Pérez-García, *Phys. Rev. Lett.* **95**, 153903 (2005).
- [18] S. Inouye, M. R. Andrews, J. Stenger, H. J. Miesner, D. M. Stamper-Kurn, and W. Ketterle, *Nature (London)* **392**, 151 (1998).
- [19] M. Theis, G. Thalhammer, K. Winkler, M. Hellwig, G. Ruff, R. Grimm, and J. H. Denschlag, *Phys. Rev. Lett.* **93**, 123001 (2004).
- [20] D. M. Stamper-Kurn, M. R. Andrews, A. P. Chikkatur, S. Inouye, H. J. Miesner, J. Stenger, and W. Ketterle, *Phys. Rev. Lett.* **80**, 2027 (1998).
- [21] J. P. Martikainen, *Phys. Rev. A* **63**, 043602 (1999).
- [22] A. G. Litvak and V. A. Mironov, *Izv. Vyssh. Uchebn. Zaved., Radiofiz.* **11**, 1911 (1968).
- [23] N. N. Akhmediev, *Sov. Phys. JETP* **56**, 229 (1982).
- [24] V. M. Pérez-García, H. Michinel, J. I. Cirac, M. Lewenstein, and P. Zoller, *Phys. Rev. Lett.* **77**, 5320 (1996).
- [25] E. M. Wright, D. R. Heatley, and G. I. Stegeman, *Phys. Rep.* **194**, 309 (1990); H. Michinel, *Int. J. Optoelectron.* **11**, 277 (1997); D. Mihalache, M. Bertolotti, and C. Sabilia, *Prog. Opt.* **27**, 229 (1989); D. Mihalache and D. Mazilu, *IEE Proc.-J:*

- Optoelectron. **138**, 365 (1991).
- [26] R. B. Diener, Biao Wu, M. G. Raizen, and Q. Niu, Phys. Rev. Lett. **89**, 070401 (2002).
- [27] S. L. Cornish, N. R. Claussen, J. L. Roberts, E. A. Cornell, and C. E. Wieman, Phys. Rev. Lett. **85**, 1795 (2000); J. L. Roberts, N. R. Claussen, S. L. Cornish, E. A. Donley, E. A. Cornell, and C. E. Wieman, Phys. Rev. Lett. **86**, 4211 (2001); E. A. Donley, N. R. Claussen, S. L. Cornish, J. L. Roberts, E. A. Cornell, and C. E. Wieman, Nature (London) **412**, 295 (2001).
- [28] T. Weber, J. Herbig, M. Mark, H. C. Nagerl, and R. Grimm, Science **299**, 232 (2003).
- [29] C. C. Bradley, C. A. Sackett, J. J. Tollett, and R. G. Hulet, Phys. Rev. Lett. **75**, 1687 (1995); C. C. Bradley, C. A. Sackett, and R. G. Hulet, *ibid.* **78**, 985 (1997).
- [30] C. Sulem and P. Sulem, *The Nonlinear Schrödinger Equation: Self-Focusing and Wave Collapse* (Springer, Berlin, 2000).